Intensity and polarization of laser-induced fluorescence due to forbidden excitation of He atoms immersed in an electric field in plasmas

K. Takiyama,[1,*] S. Furukawa,[1] S. Namba,[1] T. Oda,[2] and K. Kawasaki[3]
[1]*Graduate School of Engineering, Hiroshima University, Higashi-Hiroshima, 739-8527, Japan*
[2]*Faculty of Engineering, Hiroshima Kokusai Gakuin University, Hiroshima, 739-0321, Japan*
[3]*Science Education Section, Faculty of Education, Kochi University, Kochi, 780-8520, Japan*
(Received 20 January 2008; revised manuscript received 19 October 2008; published 4 February 2009)

Laser-induced fluorescence (LIF) processes through the Stark and electric-quadrupole moment (QDP) transitions of He I ($2\,^1S \rightarrow n\,^1D \rightarrow 2\,^1P, n=3,4$) have been investigated for reliable electric-field measurements in plasmas. A linear-polarization model is formulated for various configurations of electric fields, magnetic fields, and laser polarization. To extend the model to higher-particle-density plasmas we develop a rate-equation model involving a collisional disalignment term. Disalignment rates of $n\,^1D$ states, R_{da}, due to a collision with He gas were measured. Spatial distributions in intensity and polarization of LIF were observed in a discharge plasma. For $n=3$ with small R_{da}, the same electric-field distribution in the sheath was obtained from either of the intensity ratios of the Stark to QDP component and the polarization, and the sheath potential agreed well with that by an electric probe. For $n=4$ with large R_{da}, the distribution was also correctly obtained from partially depolarized LIF wave forms by using the extended model. These results show that our extended model provides an accurate measurement of the electric field. The minimum detectable field strength was 80 V/cm for $n=4$. Application and limitations of the methods are discussed.

DOI: 10.1103/PhysRevE.79.026402 PACS number(s): 52.70.−m, 32.60.+i, 52.80.−s, 52.20.Hv

I. INTRODUCTION

The electric field has been one of the most important plasma parameters in studies on plasma confinement [1] and plasma material interactions in magnetic fusion [2], inertial electrostatic confinement fusion [3], plasma processing [4], and electric double layers [5]. To directly and nonintrusively measure the electric fields in plasmas, laser-induced fluorescence (LIF) methods that rely on the Stark splitting and mixing [4,6–9] of atomic or molecular states have been developed. These methods have been successfully applied to low-density plasmas. The Stark splitting of high-lying Rydberg states, which is very sensitive to the electric field, will be, however, wiped out by the line broadening with increasing plasma particle density. This will also be complicated due to the Zeeman splitting under high magnetic fields. On the other hand, laser excitation of the allowed transition of atoms and molecules leads to weak forbidden fluorescence lines induced by the Stark mixing between nondegenerate energy levels. The field strength E can be determined by the ratio of forbidden to allowed line intensity [4,9]. In high-density plasmas it will be difficult to measure the forbidden line because of the disturbance due to the strong background plasma light.

It has been demonstrated that intense laser excitation of a weak Stark-induced electric-dipole moment transition (Stark transition) results in an intense field-dependent allowed fluorescence [9,10]. The LIF method combined with a technique of Li-beam probing has been applied, for the first time, to a large plasma device, RFC-XXM, to measure E distribution in the hydrogen plasma with an electron density of 3×10^{11} cm^{-3} and a magnetic field of 1.1 T [11,12]. In this measurement, however, a sophisticated procedure had to be carried out to estimate E, because there was no standard for determining E directly from the observed field-dependent fluorescence intensity.

A new *in situ* calibration method for E has been proposed by using the four level system of singlet He atoms shown in Fig. 1 [13]. Metastable He atoms ($2\,^1S$) in electric fields can be optically excited to the $n\,^1D$ (principal quantum number $n \geqslant 3$) states through both the Stark and electric-quadrupole moment (QDP) transitions (forbidden excitation). The forbidden excitation can generate a population imbalance among magnetic sublevels of the excited states, called alignment. Subsequently, the aligned atoms emit linearly polarized fluorescence [14]. Measurements of the polarized fluorescence enable us to separate the Stark and QDP components involved in LIF. Using the intensity of the QDP component as a standard of the electric field, we can determine E from either the intensity ratio of the Stark to QDP

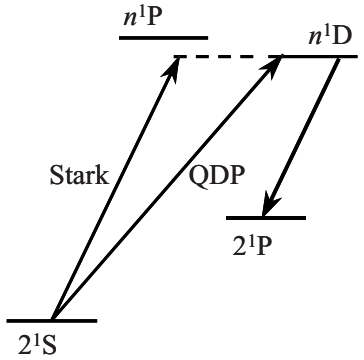

FIG. 1. Partial energy level diagram of He I for the forbidden excitation $2\,^1S \rightarrow n\,^1D$ through the Stark and QDP transitions and the subsequent fluorescence transition $n\,^1D \rightarrow 2\,^1P$ in an electric field.

*takiyam@hiroshima-u.ac.jp

component or the polarization [13]. Previously, we showed that the polarization method was applicable to the plasmas with a relatively low gas pressure of 0.3 Torr under a magnetic field of 2.5 kG [15] and the sensitivity was so high as to be comparable to that of the Stark splitting method using the high-lying Rydberg states, despite the low-lying states being used [16]. This means that the Stark mixing can provide high sensitive measurements in plasmas with high-particle density. It is, however, expected that relaxation of the population imbalance due to collisions of aligned $n\,^1D$ atoms with the plasma particles (collisional disalignment) causes a significant depolarization of LIF in such plasmas.

The aim of this work is to develop an extended method for measuring the electric field in higher-density plasmas for various configurations of electric fields, magnetic fields, and laser polarization. The experiments are carried out in a hollow cathode and a Penning discharge plasma. The gas pressure and the electron density are 0.84 Torr and 2×10^{11} cm^{-3} at the highest, respectively. The ionization degree is very low, and hence the atomic collisional processes are dominant.

In Sec. II, we present the calculated absorption coefficients of the forbidden transitions on the basis of the quasistatic approximation and a linear polarization (LP) model relating the intensity and polarization of LIF to E. We also describe a rate-equation (RE) model for studying the effect of the disalignment on the polarization. In Sec. III, the experimental details are described. In Sec. IV, the temporal behavior and spatial distribution of the polarized LIF due to the forbidden excitations are presented. The influence of the magnetic field is also examined. In Sec. V, spatial distributions of E are determined by methods of the intensity ratio of the Stark to QDP component and of the polarization according to the LP model. It should be noted that the obtained distributions by two different methods agree very well. We analyze partially depolarized LIF wave forms due to the collisional disalignment for the accurate E determination. Finally, the effect of collisional depolarization on electric-field measurements and the application to the magnetically confined plasmas are discussed in Sec. VI.

II. POLARIZED FLUORESCENCE DUE TO FORBIDDEN EXCITATION

A. Forbidden-absorption coefficients

We consider the forbidden excitation of $2\,^1S$ atoms in the configuration shown in Fig. 2(a), where the static electric field **E** and the magnetic field **B** are parallel to the z axis and the exciting laser with a linear polarization vector $\mathbf{e}_L$ is injected along the y axis. The matrix element of the electromagnetic transition (EM) from $2\,^1S$ to the perturbed $n\,^1\tilde{D}$ is given as a sum of those for the Stark-induced electric-dipole moment ($E1$) and the QDP ($E2$) transitions as follows:

$$\langle n\,^1\tilde{D}|EM|2\,^1S\rangle = c_{nP\text{-}nD}\langle n\,^1P|E1|2\,^1S\rangle + \langle n\,^1D|E2|2\,^1S\rangle. \tag{1}$$

Here, $c_{nP\text{-}nD}$ is a level-mixing coefficient given by

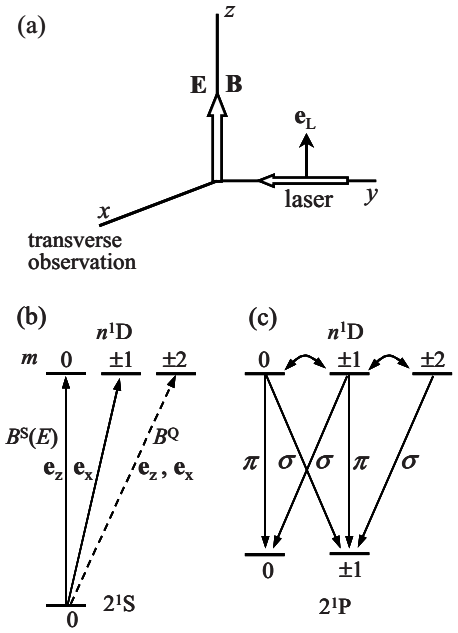

FIG. 2. (a) Excitation and observation configurations for LIF. (b) Excitation processes for the Stark (solid lines) and QDP (dashed line) transitions by laser with a linear polarization $\mathbf{e}_z$ or $\mathbf{e}_x$ under an electric field (with no magnetic field). (c) Fluorescence processes and collisional population transfers among magnetic sublevels.

$$c_{nP\text{-}nD} = eE\langle n\,^1D|z|n\,^1P\rangle/(\varepsilon_{nD}^{(0)} - \varepsilon_{nP}^{(0)}), \tag{2}$$

where $\varepsilon_{nD}^{(0)}$ ($\varepsilon_{nP}^{(0)}$) is the energy of the relevant unperturbed level. The transition probability can be obtained from the square of the matrix element. When $\mathbf{E}\perp\mathbf{B}$ geometry is considered, the Stark-QDP interference terms [17] appear in the transition probability for the optical excitation that creates another kind of population imbalance among the magnetic sublevels, called orientation. However, we are not able to detect the imbalance in the transverse observation scheme [Fig. 2(a)] under the weak magnetic field, since the interference terms are effectively canceled out. Then, the coefficient of the forbidden absorption can be simply written as

$$B_{2S\text{-}nD}(\mathbf{e}_L,E) = B^S(\mathbf{e}_L,E) + B^Q(\mathbf{e}_L), \tag{3}$$

where $B^S(\mathbf{e}_L,E)$ and $B^Q(\mathbf{e}_L)$ denote the Stark and QDP components, respectively [Fig. 2(b)]. The coefficient (cm^2 erg^{-1} s^{-1}) of the Stark transition is given by

$$B^S(\mathbf{e}_L,E) = \frac{8\pi^3c^2}{\hbar\omega^3}|c_{nP\text{-}nD}|^2A_{nP\text{-}2S}(\mathbf{e}_L), \tag{4}$$

where $|c_{nP\text{-}nD}|^2$ is the probability that the perturbed $\tilde{D}$ stays in the unperturbed P and $A_{nP\text{-}2S}$ is the probability of the spontaneous transition $n\,^1P\rightarrow 2\,^1S$. The coefficients were calculated as a function of E for the laser light polarized parallel ($\mathbf{e}_z$) and perpendicular ($\mathbf{e}_x$) to **E** according to Ref. [10]. The dependences on E were quadratic when $E<100$ kV/cm for $n=3$ and $E<6$ kV/cm for $n=4$. Thus, the dependence can be written as

TABLE I. Absorption coefficients of the Stark and QDP transitions ($2\ ^1S \rightarrow n\ ^1D$) with $\Delta m=0, \pm 1$, and ± 2.

Geometry	Absorption coefficients ($cm^2\ erg^{-1}\ s^{-1}$)	$n=3$	$n=4$	Δm
E$\|$**z**, **B**$\|$**z**	$B^S(\mathbf{e}_z, 1\ kV/cm)$	2.7×10^4	1.6×10^5	0
	$B^S(\mathbf{e}_x, 1\ kV/cm)$	2.0×10^4	1.2×10^5	±1
	$B^Q(\mathbf{e}_z)$	8.15×10^4	8.9×10^3	±1
	$B^Q(\mathbf{e}_x)$	8.15×10^4	8.9×10^3	±2
E$\|$**x**, **B**$\|$**z**	$B^S(\mathbf{e}_z, 1\ kV/cm)$	2.0×10^4	1.2×10^5	±1
	$B^S(\mathbf{e}_x, 1\ kV/cm)$	$(1/4)\times2.7\times10^4$	$(1/4)\times1.6\times10^5$	0
		$(3/4)\times2.7\times10^4$	$(3/4)\times1.6\times10^5$	±2
	$B^Q(\mathbf{e}_z)$	8.15×10^4	8.9×10^3	±1
	$B^Q(\mathbf{e}_x)$	8.15×10^4	8.9×10^3	±2

$$B^S(E) = B^S(1\ \mathrm{kV/cm})E^2, \tag{5}$$

where $B^S(1\ kV/cm)$ stands for the value at $E=1\ kV/cm$. On the other hand, the absorption coefficient of the QDP transition ($2\ ^1S \rightarrow n\ ^1D$) was also calculated according to Refs. [18,19]. In the calculation the radial integrals were evaluated within the Coulomb approximation and atomic data were quoted from Ref. [20]. These calculated values, $B^{S,Q}(\mathbf{e}_z)$ and $B^{S,Q}(\mathbf{e}_x)$, are summarized along with the selection rules for the corresponding transitions in Table I.

B. Linear-polarization model without collisional disalignment

Under low-density laser excitation of $2\ ^1S$ atoms, the population density of $n\ ^1D$ is proportional to the pumping rate, $\rho_L B_{2S\text{-}nD}$, as follows:

$$n_{nD}(z,E) \propto n_{2S}(z)\Delta t_L \rho_L(\mathbf{e}_L) B_{2S-nD}(\mathbf{e}_L, E), \tag{6}$$

where $n_{2S}(z)$ is the population density of $2\ ^1S$ at a given position z, Δt_L is the laser pulse width, and $\rho_L(\mathbf{e}_L)$ is the laser power density (erg/cm^2). In the geometry of **B**$\|$**E**$\|$**z**, since the quantization axis is along **B**, the atoms are excited through the Stark transition to the sublevels $m=0$ and ±1 of $n\ ^1D$ by the laser with $\mathbf{e}_z$ and $\mathbf{e}_x$, while through the QDP transition to the sublevels $m=\pm1$ and ±2, respectively [21].

The excited atoms emit fluorescence ($n\ ^1D \rightarrow 2\ ^1P$) with intensity given as functions of z and E as follows:

$$I(z,E) = n_{nD}(z,E)\frac{A_{nD\text{-}2P}}{\tau_{nD}(z)^{-1}}, \tag{7}$$

where $\tau_{nD}(z)^{-1}$ is the deexcitation rate of $n\ ^1D$. The intensity includes the Stark I^S and QDP I^Q components, which are defined by the subcomponents of π and σ transitions as follows:

$$I^S = I^S_\pi + 2I^S_\sigma, \quad I^Q = I^Q_\pi + 2I^Q_\sigma. \tag{8}$$

In the transverse observation along the x axis, the π and σ light intensities are given in terms of Wigner's $3j$ symbols [21] as follows:

$$I^{S,Q}_\pi = a\sum_{m_u} n^{S,Q}_u(m_u)\sum_{m_\ell}\begin{pmatrix} j_u & 1 & j_\ell \\ -m_u & 0 & m_\ell \end{pmatrix}^2,$$

$$I^{S,Q}_\sigma = \frac{1}{2}a\sum_{m_u} n^{S,Q}_u(m_u)\sum_{m_\ell}\begin{pmatrix} j_u & 1 & j_\ell \\ -m_u & \pm1 & m_\ell \end{pmatrix}^2, \tag{9}$$

where a is a constant, the value of $1/2$ is a geometric factor for the σ light, subscripts u and ℓ mean "upper" and "lower" states associated with the fluorescence transition, respectively, and $n^{S,Q}_u(m_u)$ is the population density of a given magnetic sublevel m_u in $n\ ^1D$ produced by the Stark or QDP excitation.

The polarization is written as

$$P = \frac{I_z - I_y}{I_z + I_y}. \tag{10}$$

Here, I_z and I_y are linearly polarized components observed in the experiments, which consist of two subcomponents due to the Stark and the QDP transitions as follows:

$$I_z = I^S_z + I^Q_z, \quad I_y = I^S_y + I^Q_y. \tag{11}$$

The relations between the subcomponents are given by

$$I^S_z = r^S_{zy} I^S_y, \quad I^Q_z = r^Q_{zy} I^Q_y. \tag{12}$$

Here, r^S_{zy} and r^Q_{zy} stand for the intensity ratios, which can be estimated from the $3j$ symbols according to the selection rules. Using Eqs. (11) and (12), Eq. (10) is rewritten as

$$P = \frac{(r^S_{zy}-1) + (r^Q_{zy}-1)(I^Q_y/I^S_y)}{(r^S_{zy}+1) + (r^Q_{zy}+1)(I^Q_y/I^S_y)}. \tag{13}$$

On the other hand, the ratio of $B^S(E)$ to B^Q is related to the intensity ratio of the Stark to QDP component as follows:

$$B^R(E) = \frac{B^S(E)}{B^Q} = \frac{I^S_\pi + 2I^S_\sigma}{I^Q_\pi + 2I^Q_\sigma} = \frac{(r^S_{\pi\sigma}+2)I^S_\sigma}{(r^Q_{\pi\sigma}+2)I^Q_\sigma}. \tag{14}$$

where $r^S_{\pi\sigma}=I^S_\pi/I^S_\sigma$ and $r^Q_{\pi\sigma}=I^Q_\pi/I^Q_\sigma$. In this geometry [Fig. 2(a)], since I^Q_y/I^S_y in Eq. (13) is identical with I^Q_σ/I^S_σ in Eq. (14), we finally obtain the following relationship between P and $B^R(E)$:

TABLE II. Quantization axes, magnetic sublevels populated by the laser excitation, and fluorescence intensity ratios of subcomponents associated with Stark ($E1$) and QDP ($E2$) transitions in respective configurations of eight cases. The intensity ratio with an asterisk does not change due to the collisional disalignment, because both I_z^S (I_z^Q) and I_y^S (I_y^Q) in the ratio are σ components when the quantization axis points to the x direction.

			Stark transition ($E1$)				QDP transition ($E2$)			
Case	Configuration		$\mathbf{q}^S$	m	$r_{\pi\sigma}^S$	r_{zy}^S	$\mathbf{q}^Q$	m	$r_{\pi\sigma}^Q$	r_{zy}^Q
A(z)	$\mathbf{E}\|\mathbf{z}$	$\mathbf{e}_z$	$\mathbf{z}$	0	4	4	$\mathbf{x}$	±2	0 ($=r_{xy}^Q$)	1*
A(x)	$\mathbf{E}\|\mathbf{z}$	$\mathbf{e}_x$	$\mathbf{z}$	±1	2	2	$\mathbf{z}$	±2	0	0
B(z)	$\mathbf{E}\|\mathbf{B}\|\mathbf{z}$	$\mathbf{e}_z$	$\mathbf{z}$	0	4	4	$\mathbf{z}$	±1	2	2
B(x)	$\mathbf{E}\|\mathbf{B}\|\mathbf{z}$	$\mathbf{e}_x$	$\mathbf{z}$	±1	2	2	$\mathbf{z}$	±2	0	0
C(z)	$\mathbf{E}\|\mathbf{x}$	$\mathbf{e}_z$	$\mathbf{x}$	±1	2 ($=r_{xy}^S$)	1*	$\mathbf{x}$	±2	0 ($=r_{xy}^Q$)	1*
C(x)	$\mathbf{E}\|\mathbf{x}$	$\mathbf{e}_x$	$\mathbf{x}$	0	4 ($=r_{xy}^S$)	1*	$\mathbf{z}$	±1	0	0
D(z)	$\mathbf{E}\|\mathbf{x}$, $\mathbf{B}\|\mathbf{z}$	$\mathbf{e}_z$	$\mathbf{z}$	±1	2	2	$\mathbf{z}$	±1	2	2
D(x)	$\mathbf{E}\|\mathbf{x}$, $\mathbf{B}\|\mathbf{z}$	$\mathbf{e}_x$	$\mathbf{z}$	0, ±2	0.4	0.4	$\mathbf{z}$	±2	0	0

$$P = \frac{B^R(E)(r_{\pi\sigma}^Q+2)(r_{zy}^S-1)+(r_{zy}^Q-1)(r_{\pi\sigma}^S+2)}{B^R(E)(r_{\pi\sigma}^Q+2)(r_{zy}^S+1)+(r_{zy}^Q+1)(r_{\pi\sigma}^S+2)}. \quad (15)$$

When $B=0$, the quantization axis for the QDP transition is strongly dependent upon the laser polarization. The direction is always perpendicular to the polarization plane of the laser, because the QDP interacts only with the spatial gradient of the laser electric field [22]. Therefore, $r_{\pi\sigma}^S=r_{zy}^S$ and $r_{\pi\sigma}^Q=r_{xy}^Q$ for the $\mathbf{e}_z$ excitation, and $r_{\pi\sigma}^S=r_{zy}^S$ and $r_{\pi\sigma}^Q=r_{zy}^Q$ for the $\mathbf{e}_x$ excitation.

Equation (15) can also be applied to the geometry of $\mathbf{B}\|\mathbf{z}$ and $\mathbf{E}\|\mathbf{x}$, using the following relations: $r_{\pi\sigma}^S=r_{zy}^S$ and $r_{\pi\sigma}^Q=r_{zy}^Q$ for either of the $\mathbf{e}_z$ and $\mathbf{e}_x$ excitations. When $B=0$, $r_{\pi\sigma}^S=r_{xy}^S$ and $r_{\pi\sigma}^Q=r_{xy}^Q$ for the $\mathbf{e}_z$ excitation, and $r_{\pi\sigma}^S=r_{xy}^S$ and $r_{\pi\sigma}^Q=r_{zy}^Q$ for the $\mathbf{e}_x$ excitation. These values for eight different configurations (eight cases) estimated from the $3j$ symbols are summarized in Table II, where the quantization axes and magnetic sublevels in $n\,^1D$ populated by the laser excitation are also listed for the Stark and QDP transitions.

When Eq. (5) is valid, the ratio $B^R(E)$ is rewritten by introducing a constant E^Q that means the electric-field strength for $B^S(E)=B^Q$:

$$B^R(E) = \frac{B^S(1\ \mathrm{kV/cm})}{B^Q}E^2 = \frac{1}{(E^Q)^2}E^2. \quad (16)$$

The values of E^Q for $\mathbf{e}_L\|\mathbf{E}$ and $\mathbf{e}_L\perp\mathbf{E}$ were obtained to be 1.7 kV/cm and 2.0 kV/cm for $n=3$ and 0.24 kV/cm and 0.28 kV/cm for $n=4$, respectively, from Table I. From Eqs. (15) and (16), E can be given as a function of P. The expressions in the cases A(z) and D(x) are given by

$$E = E^Q\sqrt{\frac{6P}{3-5P}} \quad (0 \leqslant P < 3/5), \quad (17)$$

and

$$E = E^Q\sqrt{\frac{6(1+P)}{-(3+7P)}} \quad (-1 \leqslant P < -3/7), \quad (18)$$

respectively.

C. Rate-equation model with collisional disalignment

The alternative expression of P is the longitudinal alignment A_L of the emitted radiation defined as

$$A_L = |(I_\pi - I_\sigma)/(I_\pi + 2I_\sigma)|. \quad (19)$$

The gradient of the logarithmic plot of A_L versus time yields the disalignment rate R_{da}, which represents the decay rate of the alignment of the excited atoms [14]. When R_{da} becomes considerably large and exceeds a critical rate (see Sec. VI), the anisotropy can decay before the fluorescence is emitted, and then A_L ($|P|$) will significantly decrease. As a result, it will become difficult to estimate E straightforwardly from the experimental A_L (P).

To evaluate E correctly from the partially depolarized LIF wave forms, we employ the RE model involving the disalignment process. Assuming that the disalignment is caused by the collisional population transfers (collisional transfer) between adjacent magnetic sublevels m and m' of $n\,^1D$ with $\Delta m=\pm1$ [Fig. 2(c)], and each of the transfer rates $R(m,m')$, is given by a rate C_d, the rate equation for the sublevel population density n_m is written as

$$\frac{dn_m}{dt} = -n_m\left[\sum_k A_{mk} + \sum_k n_{e,a}\langle\sigma_{e,a}v\rangle_{mk} + \sum_{m'} R(m,m')\right] + \left[\sum_k n_k A_{km} + \sum_k n_k n_{e,a}\langle\sigma_{e,a}v\rangle_{km}\right] + \sum_{m'} n_{m'}R(m',m) + \rho_L(t)(n_{2S}B_{2S\to m} - n_m B_{m\to 2S}), \quad (20)$$

where A_{mk} is the radiative transition probability from m to k; $n_{e,a}$ is the electron or atom density, and $\langle\sigma_{e,a}v\rangle_{mk}$ is the collisional transition rate coefficient. The rates for excitation, deexcitation, ionization, and recombination by electron impact are calculated according to Ref. [23]. For the atomic collisional processes, the excitation transfers between $n\,^1D$ and adjacent excited states are considered [24,25]. The last term corresponds to laser pumping of $2\,^1S$ to the sublevel m of $n\,^1D$, where $\rho_L(t)$ is the time profile of laser power density, and $B_{2S\to m}$ ($B_{m\to 2S}$) is the absorption (emission) coefficient of the forbidden transition. In the calculation, the popu-

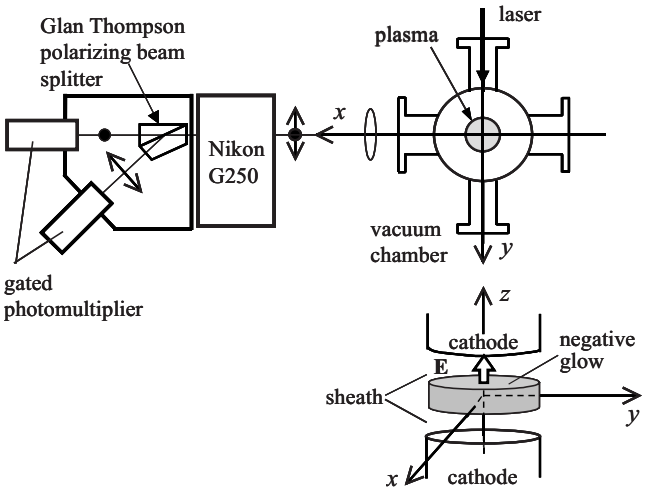

FIG. 3. Schematic view of the spectroscopic system to observe polarized components of LIF and the plane-parallel hollow-cathode plasma.

lation density is assumed to be uniformly distributed. We also assume that our plasma is optically thin except for the transitions of $n\,^1P$ to $1\,^1S$. Numerical integration of the coupled rate equations for 35 energy levels of He I ($n=1-6$) and an ionized level is performed with the Runge-Kutta method. Temporal behaviors of the π (I_z) and σ (I_y) components of LIF are reconstructed from the calculated sublevel populations in $n\,^1D$ and the instrumental time response function of the LIF detection system.

III. EXPERIMENTS

A schematic view of the spectroscopic system is shown in Fig. 3. The hollow cathode helium plasma was produced between a pair of plane-parallel disk electrodes which had a diameter of 40 mm and the separation between them was 11 mm. The discharge was performed with a He gas pressure of 0.7 Torr at a dc voltage of 170 V and a current of 40 mA. The electron temperature T_e, electron density n_e, and plasma potential in the middle of the negative glow were measured with a Langmuir probe to be 1.3 eV, 2×10^{11} cm^{-3}, and 26 V, respectively. An ion sheath with a width of approximately 2 mm was formed near each cathode surface. The electric-field direction in the sheath is along the z axis, perpendicular to the cathode surface. The origin of the z axis is specified to be the center of the gap. The magnetic field of 0–2.5 kG can be applied to the plasma along the z axis by changing the separation of a pair of permanent magnet disks.

Metastable He atoms ($2\,^1S$) were excited to $3\,^1D$ ($4\,^1D$) by a 504.2 nm (397.2 nm) light from a YAG pumped dye laser (Spectra Physics GCR-11, PDL-3) with a pulse width of 4 ns, a spectral width of 4 pm, and an output power of $\leqslant$0.5 mJ, which was weak to ensure the proportionality of the excitation with respect to the incident power. A linearly polarized laser beam was introduced into the plasma along the y axis and the polarization was adjusted to be parallel or perpendicular to the z axis by rotating a $1/2\,\lambda$ plate about the y axis. The beam had a cross section of 0.2×3 mm^2 at the plasma center. The fluorescence with a wavelength of 667.8 nm ($3\,^1D\rightarrow2\,^1P$) or 492.2 nm ($4\,^1D\rightarrow2\,^1P$) was observed along the x axis with an observation volume of 6.0 mm^3 and a solid angle of 7.2×10^{-3} sr. The linearly polarized components I_z and I_y, which were parallel and perpendicular to the z axis, respectively, were measured with a Glan-Thompson polarizing beam splitter, a 25 cm monochromator, and two photomultipliers (Hamamatsu R5322). The output signals were averaged over 500–1000 shots with a 2.5 GS/s digitizing oscilloscope. The experimental P and A_L were obtained using Eqs. (10) and (19), respectively.

The spatial distribution of LIF was measured as a function of the distance z from the center with a spatial resolution of 0.2 mm, limited by the entrance slit width of the monochromator, by finely moving the discharge vessel along the z axis. The exciting laser power was kept constant during the measurements. The distribution of the metastable atom density n_{2S} was measured by the same LIF technique as that described in Ref. [26].

On the other hand, the pressure dependence of the disalignment rate was also measured over a wide range of He gas pressures P_{He} from 5 to 840 mTorr under the constant discharge current of 25 mA. Low-pressure plasmas ($P_{\mathrm{He}}<200$ mTorr) were produced by a Penning-discharge device consisting of a pair of ring cathodes (20 mm i.d.) with a gap of 70 mm and a cylindrical anode (30 mm i.d., 60 mm length) coaxially set in the gap. A magnetic field of 400 G was applied along the electrode axis by Helmholtz coils. The values of T_e and n_e were 0.8 eV and 1.1×10^{11} cm^{-3} at the center of the plasma operated at 10 mTorr, respectively. Higher-pressure plasmas ($P_{\mathrm{He}}\geqslant200$ mTorr) were produced by the hollow cathode discharge.

IV. EXPERIMENTAL RESULTS

A. Intensity and polarization of LIF

LIF ($4\,^1D\rightarrow2\,^1P$) polarization components were observed in the hollow cathode plasma produced at $P_{\mathrm{He}}=0.7$ Torr and $B=0$. Figure 4(a) shows the wave forms at $z=3.7$ mm in the boundary region between the negative glow and the sheath, where the electric field is negligibly weak. In the case of the $\mathbf{e}_z$ excitation, the LIF is unpolarized: the time evolution of $I_z(\mathbf{e}_z)$ is the same as that of $I_y(\mathbf{e}_z)$ within the whole time range. This can be reasonably explained if the fluorescence is induced by the QDP excitation whose quantization axis turns toward the x direction, as mentioned in Sec. II B. Then, circularly polarized radiations due to the σ transitions ($\Delta m=\pm1$) are emitted along the observation axis (x axis). In the case of the $\mathbf{e}_x$ excitation where the quantization axis is along the z direction, the LIF is clearly polarized. The y component $I_y(\mathbf{e}_x)$ is also due to the σ transition because of having almost the same wave form and intensity as the above $I_{z,y}(\mathbf{e}_z)$. On the other hand, the z component $I_z(\mathbf{e}_x)$ is obviously different from the σ light, indicating that the signal should be due to the π-light emission ($\Delta m=0$) after the collisional transfers between magnetic sublevels of the aligned $4\,^1D$ atoms [Fig. 2(c)]. The time evolution of the polarization is shown by closed circles in Fig. 4(b). The polarization (−0.73 at $t=4$ ns) decays rapidly and disappears

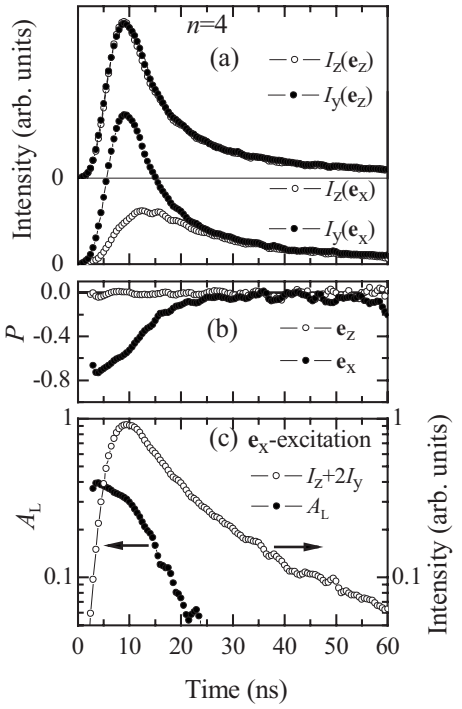

FIG. 4. Measured wave forms of (a) LIF (492.2 nm) polarized components and (b) the corresponding polarization by the $\mathbf{e}_z$ and $\mathbf{e}_x$ excitations at $z=3.7$ mm in the negative glow. (c) Time decay of the longitudinal alignment of $4\,^1D$ and LIF intensity for the $\mathbf{e}_x$ excitation.

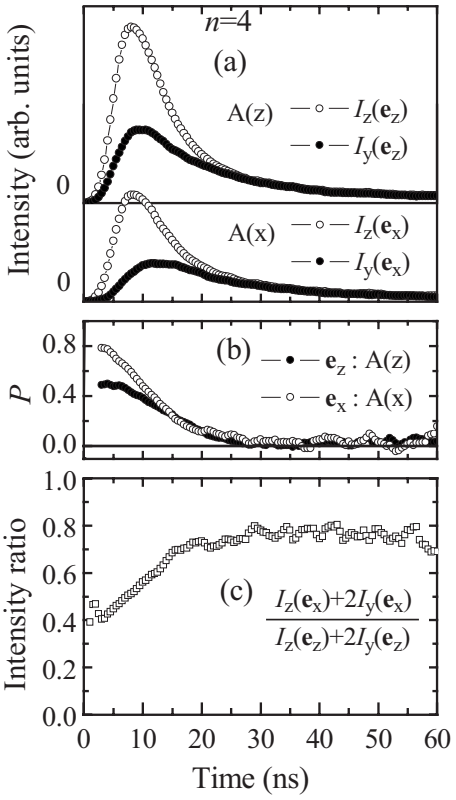

FIG. 5. Measured wave forms of (a) LIF (492.2 nm) polarized components, (b) the corresponding polarization, and (c) the ratio of LIF intensities by the $\mathbf{e}_z$ and $\mathbf{e}_x$ excitations at $z=5.0$ mm in the sheath.

around $t=25$ ns. This suggests the existence of strong depolarization by the frequent collision of aligned atoms with the plasma particles.

Figure 4(c) shows the time evolutions of the alignment A_L and the intensity $I_\pi+2I_\sigma$ for the $\mathbf{e}_x$ excitation. The alignment decays exponentially from 10 ns (laser-off time) to 20 ns. From the time constant τ_{LA} of 7.0 ns, the disalignment rate R_{da} was estimated to be 1.4×10^8 s^{-1}. On the other hand, the time decay in intensity has two components. From the fast component (mean lifetime $\tau_{4D}=11$ ns), the decay rate was estimated to be 9.1×10^7 s^{-1}, which was much larger than the radiative transition probability for the 492.2 nm fluorescence (2.0×10^7 s^{-1}). Such effective deexcitation is dominated by excitation transfers from $4\,^1D$ towards $4\,^1P$ and $4\,^1F$ due to the collision of the $4\,^1D$ atoms with the ground state He atoms rather than electrons because of the low electron density in this boundary region. After a kink at 20 ns, the intensity shows slow decay that may be responsible for the reverse processes.

Similarly, we observed the wave forms of the LIF ($3\,^1D\rightarrow2\,^1P$) polarization components. For the $\mathbf{e}_x$ excitation, the polarization ($P=-0.9$) was very close to perfect polarization (-1) at the early stage and the decay rate $R_{\mathrm{da}}=9.1\times10^7$ s^{-1} ($\tau_{\mathrm{LA}}=11$ ns) was smaller than the one for $n=4$. The intensity decayed exponentially with τ_{3D} of 16 ns over a decade ($\tau_{3D}^{-1}=6.3\times10^7$ s^{-1}). This shows that the radiative transition probability (6.4×10^7 s^{-1}) is much larger than the collisional deexcitation rate, and hence the effect of the reverse processes is negligibly small.

In the sheath ($z=5.0$ mm) where the strong electric field was present, we observed the wave forms of the LIF intensity and polarization due to the Stark excitation for $n=4$, as shown in Figs. 5(a) and 5(b). The intensities relative to $I_z(\mathbf{e}_z)$ and the corresponding P, at 4 ns when the depolarization is relatively small, are listed in Table III. The intensity $I_y(\sigma)$ observed in the case of the $\mathbf{e}_x$ excitation is less than half the theoretical intensity, and consequently, the value of P becomes anomalously large. The ratio $[I_z(\mathbf{e}_x)+2I_y(\mathbf{e}_x)]/[I_z(\mathbf{e}_z)+2I_y(\mathbf{e}_z)]$ shows a smaller value of 0.4 at the onset, which gradually increases and finally reaches a constant value of 0.77 ± 0.03 at 20 ns [Fig. 5(c)]. This value agrees well with the ratio of 0.75 deduced from the Stark absorption coefficients in Table I. This means that the population is not correctly reflected in the LIF intensity at the onset of the pulse signals although normally created immediately after laser irradiation ($\mathbf{e}_x$ excitation). In other words, the σ light from the sublevels $m=\pm1$ might be depressed for 20 ns after the irradiation, and a lowering in intensity occurs. This is supported by the fact that the experimental intensity of π light

TABLE III. Relative intensity and polarization of the Stark components of LIF ($4\,^1D\rightarrow2\,^1P$) observed in the sheath ($z=5.0$ mm). Values in parentheses are theoretical.

Laser polarization	I_z (π)	I_y (σ)	P
(a) $\mathbf{e}_z$ [case A(z)]	1.0 (1)	0.31 (0.25)	0.53 (0.60)
(b) $\mathbf{e}_x$ [case A(x)]	0.61 (0.56)	0.09 (0.28)	0.74 (0.33)

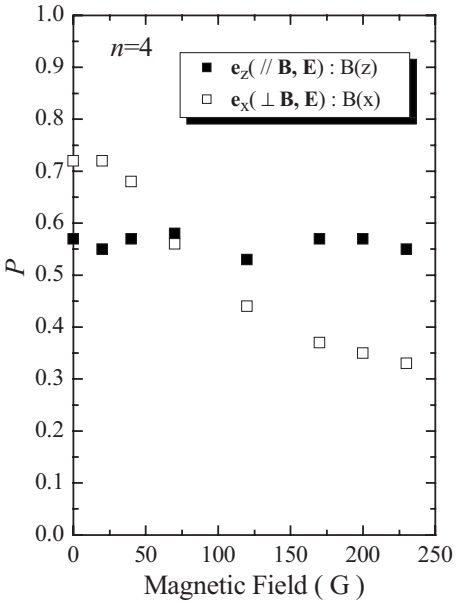

FIG. 6. Magnetic field dependences of LIF polarization measured at $z=5.0$ mm in the sheath for the $\mathbf{e}_z$ and $\mathbf{e}_x$ excitations.

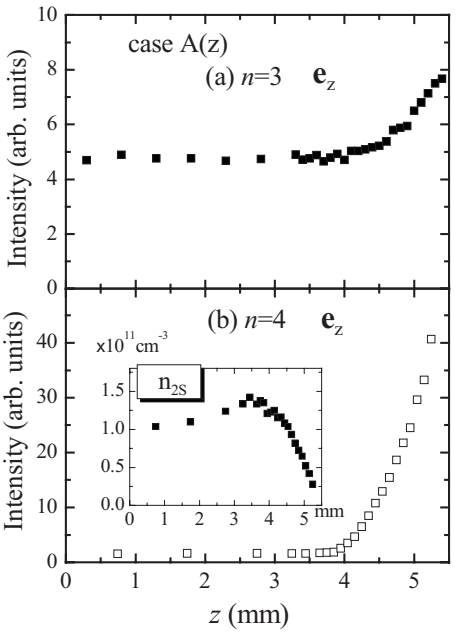

FIG. 7. Spatial distributions of time-integrated LIF intensities measured for (a) $n=3$ and (b) $n=4$ by the $\mathbf{e}_z$ excitation. The intensities are normalized to the density of metastable He ($2\,^1S$) atoms depicted in the inset. The cathode surface is situated at $z=5.5$ mm.

from the same sublevels agreed with the theoretical one (see Table III). For $n=3$, the σ-light depression was also found but this was considerably smaller than that for $n=4$.

The decay rates of the intensity and alignment, τ_{nD}^{-1} and R_{da}, obtained for $n=3$ and 4 in the sheath were in good agreement with those in the boundary region. Therefore, it is evident that the dominant collision process is atomic in this experiment.

B. Influence of magnetic field on LIF polarization

We have already demonstrated that in the negative glow (E is negligibly weak) the quantization axis of QDP is dominated by the interaction with the laser electric field for weak B while the higher B directs the axis in Ref. [27].

In this work, the dependence of P of 492.2 nm LIF due to the Stark excitation on the magnetic field ($\mathbf{B}\|\mathbf{E}$) was investigated in the sheath ($z=5.0$ mm). The results are shown in Fig. 6. In the case of the $\mathbf{e}_z$ excitation, the values of P are kept almost constant with respect to B and are in good agreement with the theoretical value of 0.6 estimated for the case B(z) (see Table II). In the case of the $\mathbf{e}_x$ excitation, the measured P shows a large value of 0.72 at a lower B (0–20 G). With further increasing B the value gradually decreases approaching ~0.3, which is very close to the theoretically expected value of 1/3 for the case B(x). This value remained up to $B=2.5$ kG. It should be emphasized that the σ-light depression mentioned above disappeared under high magnetic fields. This σ-light depression can be qualitatively explained to be responsible for an interference between σ^+ and σ^- radiations caused by a coherent superposition of the eigenstates ($m=+1$ and -1 in $4\,^1D$) [28], since the spectral width of the pump radiation is broader than the Zeeman splitting between sublevels of $m=+1$ and -1 in the present experiments. The disappearance of the depression found after $t=20$ ns at $B=0$ [see Fig. 5(c)] can also be understood as a result of relaxation of the coherency produced by the laser excitation due to frequent atomic collisions.

C. Spatial distribution of LIF intensity and polarization

Figure 7 shows the spatial distributions of the time-integrated intensity of I_z+2I_y for (a) 667.8 nm LIF and (b) 492.2 nm LIF measured for the case A(z). The intensity was normalized to the metastable atom density n_{2S}. Both LIF intensities have almost constant distributions in the negative glow. The distribution is considered to be mainly due to the QDP component, because microelectric fields generated by ions are negligibly weak in the present plasma. In the sheath region, from $z\approx 4$ mm to the cathode surface, the distributions show parabolic enhancement due to the Stark components induced by the sheath electric field. Therefore, the intensity ratio of the Stark to QDP component should be compared to that of the theoretical absorption coefficients shown in Table I. The constant components, however, do not give the QDP component correctly since the quantization axis points to the x direction for the $\mathbf{e}_z$ excitation, i.e., I_z+2I_y corresponds to $I_\sigma+2I_\sigma$. Therefore, the component I^Q was obtained by the $\mathbf{e}_x$ excitation.

Figure 8(a) shows the spatial distribution of P for the $\mathbf{e}_z$ excitation [case A(z)] of the $n=3$ system. The value of P is zero in the negative glow (from $z=0$ to 3.7 mm), and increases monotonously toward the cathode surface. On the other hand, for $n=4$ the value rapidly increases with z in the sheath and saturates near the cathode surface, as in Fig. 8(b). This saturation behavior means that the LIF due to the Stark transition is much stronger than that due to the QDP. For the $\mathbf{e}_x$ excitation [case A(x)], P in the negative glow is close to the theoretical value of the QDP component (−1), while in

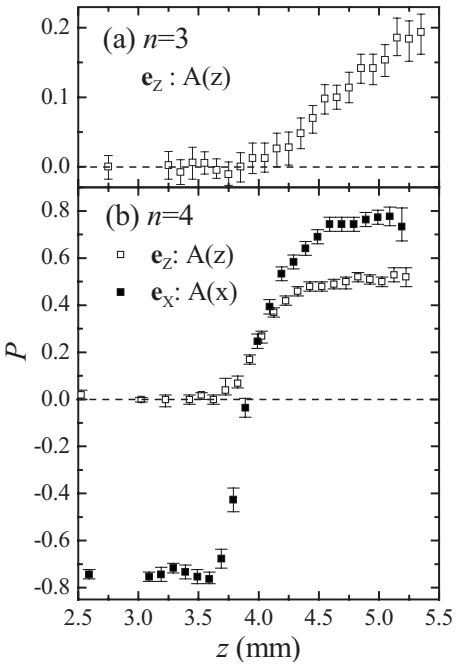

FIG. 8. Spatial distributions of LIF polarization measured for (a) $n=3$ by the $\mathbf{e}_z$ excitation and (b) $n=4$ by the $\mathbf{e}_z$ and $\mathbf{e}_x$ excitations. The cathode surface is situated at 5.5 mm.

the sheath it increases steeply to reach 0.8, which is 2.4 times as large as the theoretical value (1/3). This enhancement is due to the σ-light depression, as mentioned in Secs. IV A and IV B.

D. Pressure dependence of disalignment rate

Linearly polarized LIF due to the QDP excitation was observed with changing P_{He} from 5 to 840 mTorr. The measured disalignment rates are plotted against P_{He} for $n=4$ in Fig. 9. In the higher P_{He} region, the rate decreases linearly

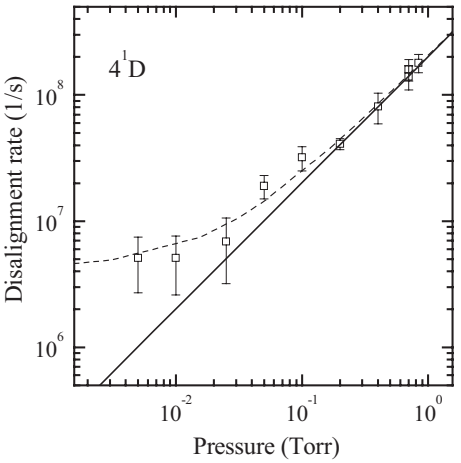

FIG. 9. Measured disalignment rates of $4\,{}^1D$ as a function of He gas pressure (open squares). A broken line is the result of the linear fit to the experimental rates. The pressure dependence of the atomic collisional rate was obtained by subtracting the electronic rate from the observed ones, as shown by a solid line.

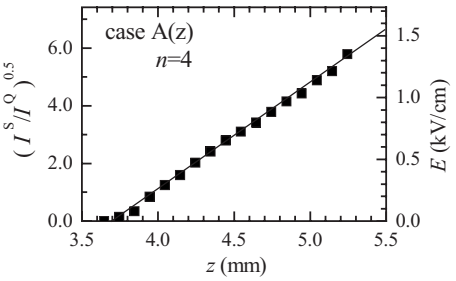

FIG. 10. Spatial distributions of the electric field deduced from the LIF intensity ratios measured for $n=4$.

with decreasing P_{He}, while in the lower region gradually approaches a constant rate responsible for electron collisions. The rates due to electron collisions were estimated to be $(2.2\pm0.8)\times10^6$ s^{-1} for $n=3$ and $(4.3\pm1.8)\times10^6$ s^{-1} for $n=4$, by extrapolating the linear-fit lines to $P_{\mathrm{He}}=0$. Finally, the linear dependence of the rates due to atom collisions on P_{He} was obtained by subtracting the electronic rate from the experimental ones, as shown by a solid line. The rate coefficients were deduced to be $(3.5\pm1.5)\times10^{-9}$ cm^3/s for $n=3$ and $(6.3\pm2.0)\times10^{-9}$ cm^3/s for $n=4$ by assuming a gas temperature of 300 K. The cross sections were also estimated to be $(2.0\pm0.8)\times10^{-14}$ cm^2 and $(3.6\pm1.1)\times10^{-14}$ cm^2, respectively, and were in fairly good agreement with those by the Hanle effect method [29].

V. ANALYSIS

A. Determination of E from the LIF intensity ratio

From Eqs. (6) and (7) the normalized LIF intensity (Fig. 7) is considered to be dependent only on $B_{2S\text{-}nD}(E)$ in the sheath and the negative glow near the sheath where the experimental $\tau_{nD}(z)$ is constant. The Stark component I^S can be extracted by subtracting the constant component I (z_{BR}, 0) observed in the boundary region (BR) between the negative glow and the sheath from the normalized intensity. Using I^Q observed at z_{BR} by the $\mathbf{e}_x$ excitation, we obtain the intensity ratio as a function of z by

$$I^S/I^Q = [I(z,E) - I(z_{\mathrm{BR}},0)]/I^Q(z_{\mathrm{BR}},0). \tag{21}$$

Since the ratio is proportional to E^2 according to the LP model in Sec. II B, the square root gives

$$E = E^Q\sqrt{I^S/I^Q}. \tag{22}$$

Figure 10 shows a typical spatial distribution of the square root of I^S/I^Q for $n=4$. Using theoretical $B^S(E)$ and B^Q, the scale of the axis was converted to E, the axis for which is shown on the right-hand side. The experimental points in the sheath show a good fit to a solid straight line according to the theoretical model given in Ref. [30]: $E(r)=(2V_C/d)(1-r/d)$, where $E(r)$ is the field strength as a function of distance r from the cathode surface, V_C is the cathode fall voltage, and d is the sheath thickness. The obtained values of d and V_C were 1.8 mm and 143 V for $n=3$, and 1.8 mm and 140 V for $n=4$, respectively. The values of V_C were in good agreement with that by the probe method

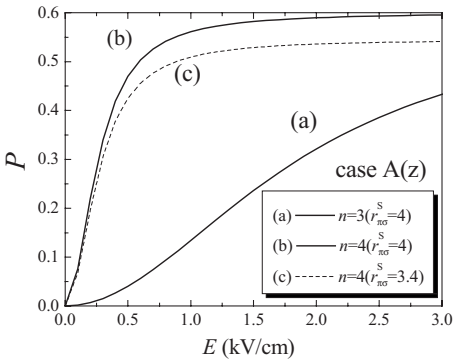

FIG. 11. Calculated LIF polarization as a function of the electric field for the case A(z).

(144 V). It was demonstrated that the theoretical ratio $B^S(E)/B^Q$ agreed well with the corresponding experimental intensity ratio, i.e., the value of E was correctly determined from the experimental I^S by using the corresponding I^Q as a standard.

B. Determination of E from LIF polarization

Figure 11 shows the calculated relationships between P and E (P-E curve) by Eqs. (15) and (16) and Table II. Using the P-E curve (a), we obtained the distribution of E in the sheath from that of P observed for $n=3$, as shown in Fig. 12(a). A straight line is the best fit to the experimental data points. The values of d and V_C were obtained to be 1.8 mm and 140 ± 10 V, respectively. It should be emphasized that V_C is in good agreement with that evaluated from the intensity ratio. This also shows that there is no major effect of the collisional disalignment on the determination of E for $n=3$. For $n=4$, however, the experimental P of 0.52 at $z=5.2$ mm [Fig. 8(b)], where $E=1.3$ kV/cm [Figs. 10 and 12(a)], is smaller than the expected one (~ 0.58) from the P-E curve (b). It is considered that this small reduction in P is caused by the depolarization effect on the intensity ratio $r^S_{\pi\sigma}$, because the Stark component is a large proportion of the LIF intensity in the high-field region. The ratio was estimated to be 3.4 for $P=0.52$ at $E=1.3$ kV/cm from Eqs. (15) and (16), and then a modified P-E curve (c) was drawn in Fig. 11. Using the curve a linear dependence of E on z was obtained in the sheath region [Fig. 12(b)]. Comparison of the obtained values of d (1.8 mm) and V_C (143 ± 15 V) with those for $n=3$ indicated good agreement. Thus, it was found that the depolarization in the Stark components had a considerable effect on the determination of E, and in particular, this influence became very large in the saturation stage of the P-E curve. The above results are consistent with the fact that the experimental disalignment rate of $4\,^1D$ was 1.5 times larger than that of $3\,^1D$.

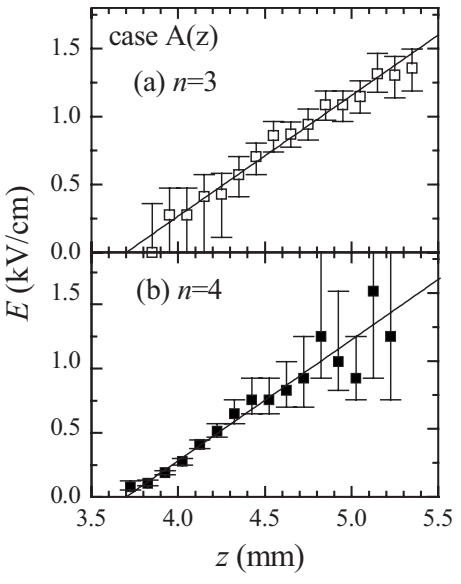

FIG. 12. Spatial distributions of the electric field deduced from the measured LIF polarization for (a) $n=3$ ($r^S_{\sigma\pi}=4$) and (b) $n=4$ ($r^S_{\sigma\pi}=3.4$).

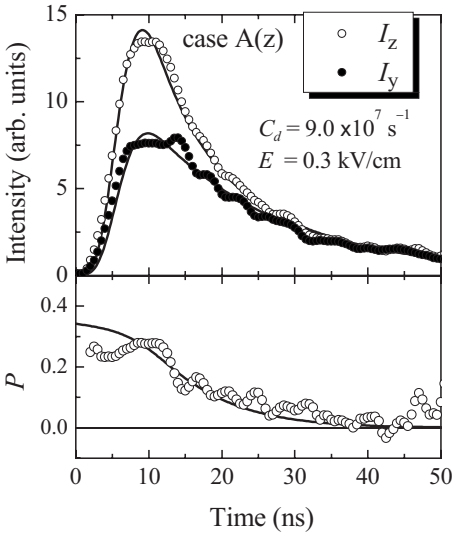

FIG. 13. Calculated LIF wave forms (solid lines) fitted to the experimental ones observed at $z=4.0$ mm in the sheath for the $\mathbf{e}_z$ excitation [case A(z)].

C. Determination of E using the rate-equation model

Figure 13 shows the wave forms of I_z, I_y, and P for $n=4$ observed at $z=4.0$ mm in the sheath region by the $\mathbf{e}_z$ excitation [case A(z)]. We analyzed the wave forms for E by using the RE model in the following procedure. First, the curve fitting was carried out for the wave forms observed by the $\mathbf{e}_x$ excitation at the boundary ($z=3.7$ mm where $E=0$) to determine the collisional transfer rate C_d, the value of which was considered to be constant in the sheath and the boundary regions (see Sec. IV A). Next, taking E as a fitting parameter and using the determined C_d, the procedure was iterated until the best-fit curves to the wave forms in Fig. 13 were obtained. Thus, C_d and E were determined uniquely to be 9.0×10^7 s^{-1} and 0.3 kV/cm, respectively. The curves are depicted by solid lines in the figure. The agreement between the experimental and the calculated decay rates of A_L was satisfactory. According to the same procedure, the spatial distribution of E between $z=3.9$ and 4.5 mm was obtained to be

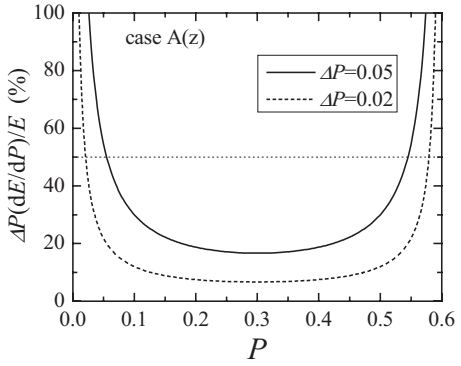

FIG. 14. Relative errors in E determination for the case A(z) when the experimental errors ΔP are 0.05 and 0.02.

in good agreement with that from the P-E curve for $r_{\pi\sigma}^{S}=3.4$ [Fig. 12(b)].

VI. DISCUSSION

A. Electric-field measurement in plasmas by LIF polarization

The polarization method has an advantage in that no calibration is required for the absolute sensitivity since the quantities n_{2S} and ρ_L in Eq. (6) are canceled out in Eq. (10). Only the measurement of P is needed to determine E. The P-E curves for various excitation and observation configurations can be calculated by Eqs. (15) and (16) and the theoretical parameters (Table II). In this work, we have demonstrated that the cases A(z), B(z), C(x), and D(x) are available for the electric-field measurements within a framework of the LP model in Sec. II B. On the other hand, we found that in the cases C(z) and D(z) P had no dependence on E, and also in the cases A(x), B(x), and C(z) the fluorescence process included the σ-light depression due to the interference between σ^+ and σ^- transitions (Sec. IV B). The case A(x), however, can provide us with a method to measure the electric fields with the most highest sensitivity among the configurations considered here, because the curve of P has the largest gradient with respect to E, as inferred from the data for A(x) in Fig. 8(b).

Based on the LP model [P-E curves (a) and (b) for A(z) in Fig. 11], we can give the uncertainty $\Delta E/E$ in the field determination as a quantity independent of the quantum number n using the theoretical dispersion dE/dP at a given P as follows:

$$\Delta E/E = \Delta P(dE/dP)_P/E, \tag{23}$$

where ΔP is the experimental error of P. In our experiment, with ΔP being 0.05, the dependence of $\Delta E/E$ on P yields a U-shaped curve, as shown by a solid line in Fig. 14, where the region showing the highest accuracy in the determination of E is around $P=0.3$. Assuming a measurable electric field to be determined within an error of 50%, we obtained the ranges to be $0.56\ \mathrm{kV/cm}<E<6.2\ \mathrm{kV/cm}$ for $n=3$ and $80\ \mathrm{V/cm}<E<880\ \mathrm{V/cm}$ for $n=4$. The ranges can be extended by decreasing the experimental errors in P, e.g., a broken line with $\Delta P=0.02$ for $n=4$ (the measurable E is approximately 50 V/cm). The use of the energy level system with higher n can also make it possible to reduce the minimum measurable E, e.g., 10 V/cm for $n=5$.

In order to apply this LIF technique to a plasma that does not contain He gas, a neutral He beam probe with a sufficient density of singlet metastable atoms is required. For plasma edge measurements in magnetic fusion devices, we have developed a supersonic He beam that can minimize the motional Stark effect [31]. The polarization method can also be applicable by use of other species, e.g., Li atoms which have a useful energy level system, $2\,^2S$-n^2D.

B. Depolarization by collisions with plasma particles

In a plasma with a higher particle density, careful treatment is necessary to determine P from the observed polarization components of LIF. It was demonstrated that the wave form analysis on the basis of the RE model was very helpful in the determination of E. There should, however, be an upper limit of the disalignment rate R_{da} for the validity of the analysis. In order to clarify the limit, the time behavior of P was simulated against R_{da} by the RE model. If $R_{\mathrm{da}}<1\times10^8\ \mathrm{s}^{-1}$, the alignment did not decay significantly at an early stage and then E was straightforwardly determined, while the wave form analysis became needed at higher R_{da}. An experiment showed that for the $n=4$ system with R_{da} of $1.4\times10^8\ \mathrm{s}^{-1}$ at 0.7 Torr E was correctly determined only by the wave form analysis. With further increasing the particle density, the difference between both polarization components in intensity decreases and finally the polarization will disappear. This tendency will significantly appear in LIF signals having small P, e.g., P in the weak E region of the case A(z) shown in Fig. 11. This results in a lowering of the detection sensitivity of E. The simulation suggested that the upper limit of the rate appeared to be around $3\times10^8\ \mathrm{s}^{-1}$ for the case A(z). From the rate coefficients of the atomic collisional disalignment, we deduced the upper limit of the gas pressure to be 3 Torr for $n=3$ and 2 Torr for $n=4$. On the other hand, the intensity ratio method has a potentiality for applying to plasmas with a high pressure exceeding the limit, because the determination of E is free from the depolarization.

C. Applications to magnetically confined plasmas

In the edge region of magnetically confined fusion plasmas, weak radial electric fields are generated perpendicular to the magnetic field. Only the case D(x) having the detection limit of approximately 70 V/cm at $\Delta P=0.05$ is suitable for $\mathbf{E}\perp\mathbf{B}$ geometry. The upper limit for the disalignment rate R_{da} in this case is much higher than in the case A(z), because $|P|$ is nearly equal to unity at the lower limit of E [cf. Eq. (18)]. From the electronic disalignment rate estimated indirectly in Sec. IV D, it was suggested that the detection limit for $n=4$ was unaffected by electron impact below n_e of $1\times10^{13}\ \mathrm{cm}^{-3}$. In such high-density plasmas, however, isotropic microfields induced by the charged particles will be comparable to the radial fields. Since the polarization method can detect both electric fields, one should evaluate the microfield strength from the local electron density to determine the radial field strength accurately.

A much stronger magnetic field in fusion devices brings about very large Zeeman splitting in atomic states. In such a case, we need to simultaneously excite two transitions, the Stark and QDP transitions, with the corresponding two-color laser system to determine E [15].

VII. SUMMARY

Absorption coefficients of the forbidden transitions of He I ($2\,^1S \rightarrow n\,^1D$, $n=3,4$) were quantum-mechanically calculated for light polarized parallel and perpendicular to the electric-field direction. Both the intensity and polarization of the fluorescence ($n\,^1D \rightarrow 2\,^1P$, $n=3,4$) induced by the forbidden excitation were theoretically related to the electric-field strength for various configurations of the electric field, magnetic field, and laser polarization [linear-polarization (LP) model without disalignment]. The LP model was extended to higher-particle-density plasmas by employing a set of coupled rate equations involving the collisional disalignment process to analyze the observed LIF wave forms for E.

We observed temporal evolutions of linearly polarized LIF due to the forbidden excitation in the sheath and negative glow region in hollow-cathode plasmas to elucidate LIF processes for the various configurations. In the case of Stark excitation by a laser light polarized linearly perpendicular to **E**, an interference due to a coherent superposition of the eigenstates was found in the σ-fluorescence process. Special attention was paid to the depolarization process caused by the collisions between particles in the plasmas. Rate coefficients for the atomic collisional disalignment dominating the process in the present plasma conditions were obtained from the He gas pressure dependence of time decay of A_L for $n=3$ and 4.

The spatial distribution of the LIF intensity observed at $P_{\mathrm{He}}=0.7$ Torr was analyzed using the calculated absorption coefficients for the electric-field distribution, from which the sheath potential difference was deduced. The potential difference was in good agreement with that measured by an electric probe. The same result was also obtained straightforwardly from the corresponding P distribution measured for the $n=3$ system with a disalignment rate below a critical one (1×10^8 s^{-1}) which was evaluated by the simulation using the RE model. These agreements demonstrated that our theoretical models gave us both the accurate intensity and polarization of LIF induced by the forbidden excitations for the measurement of the electric field. Even in the case of a larger collision effect, we also demonstrated that E was correctly determined by the wave form analysis.

Based on the present experimental and theoretical results, we showed that a measurable electric field was as low as 80 V/cm for the $n=4$ system [case A(z)]. Applications of the intensity ratio and polarization methods to plasmas with higher particle density and the limitations were discussed.

ACKNOWLEDGMENTS

This work was supported in part by a Grant-in-Aid for Scientific Research from the Ministry of Education, Science and Culture in Japan.

[1] R. J. Groebner, K. H. Burrell, and R. P. Seraydarian, Phys. Rev. Lett. **64**, 3015 (1990); K. Ida, S. Hidekuma, Y. Miura, T. Fujita, M. Mori, K. Hoshino, N. Suzuki, T. Yamauchi, and JFT-MGroup, *ibid.* **65**, 1364 (1990).

[2] A. Kirschner, V. Philipps, J. Winter, and U. Kögler, Nucl. Fusion **40**, 989 (2000).

[3] K. Yoshikawa, K. Takiyama, T. Koyama, K. Taruya, K. Massuda, Y. Yamamoto, T. Toku, T. Kii, H. Hashimoto, N. Inoue, M. Ohnishi, and H. Horiike, Nucl. Fusion **41**, 717 (2001).

[4] R. A. Gottscho, Phys. Rev. A **36**, 2233 (1987).

[5] A. Fruchtman, Phys. Rev. Lett. **96**, 065002 (2006), and references therein.

[6] G. A. Hebner, K. E. Greenberg, and M. E. Riley, J. Appl. Phys. **76**, 4036 (1994).

[7] U. Czarnetzki, D. Luggenhölscher, and H. F. Döbele, Phys. Rev. Lett. **81**, 4592 (1998).

[8] U. Rebhan, N. J. Wiegart, and H.-J. Kunze, Phys. Lett. **85A**, 228 (1981).

[9] K. Takiyama, Y. Kamiura, T. Fujita, T. Oda, H. Sakai, and K. Kawasaki, Jpn. J. Appl. Phys. **26**, 1945 (1987).

[10] K. Kawasaki, K. Takiyama, and T. Oda, Jpn. J. Appl. Phys. **27**, 83 (1988).

[11] K. Takiyama, K. Kadota, T. Oda, M. Hamamoto, T. Ohgo, Y. Kamiura, K. Adati, and J. Fujita, Rev. Sci. Instrum. **59**, 2351 (1988).

[12] K. Adati *et al.*, *Plasma Physics and Controlled Nuclear Fusion Research, Nice, 1988* (IAEA, Vienna, 1989), Vol. 2, p. 677.

[13] K. Takiyama, H. Sakai, M. Yamasaki, T. Oda, and K. Kawasaki, *Proceedings of the Sixth International Symposium on Laser-Aided Plasma Diagnostics* (Bar Harbor, Maine, 1993), p. 43.

[14] T. Fujimoto and S. A. Kazantsev, Plasma Phys. Controlled Fusion **39**, 1267 (1997).

[15] M. Watanabe, K. Takiyama, and T. Oda, Rev. Sci. Instrum. **70**, 903 (1999); M. Watanabe, Ph.D. thesis, Hiroshima University, 2000 (unpublished).

[16] M. Watanabe, K. Takiyama, and T. Oda, Jpn. J. Appl. Phys. **39**, L116 (2000).

[17] L. R. Hunter, W. A. Walker, and D. S. Weiss, Phys. Rev. Lett. **56**, 823 (1986).

[18] I. I. Sobelman, *Atomic Spectra and Radiative Transitions*, 2nd ed. (Springer-Verlag, 1992).

[19] P. R. Fontana, *Atomic Radiative Processes* (Academic Press, New York, 1982).

[20] W. C. Martin, J. Phys. Chem. Ref. Data **2**, 257 (1973).

[21] R. D. Cowan, *The Theory of Atomic Structure and Spectra* (University of California Press, Berkeley, 1981).

[22] B. W. Shore, *The Theory of Coherent Atomic Excitation* (Wiley-Interscience, New York, 1990), Vol. 1.

[23] T. Fujimoto, J. Quant. Spectrosc. Radiat. Transf. **21**, 439

(1979).
[24] B. Dubreuil and A. Catherinot, Phys. Rev. A **21**, 188 (1980).
[25] A. Catherinot and B. Dubreuil, Phys. Rev. A **23**, 763 (1981).
[26] K. Takiyama, H. Sakai, M. Yamasaki, and T. Oda, Jpn. J. Appl. Phys. **33**, 5038 (1994).
[27] K. Takiyama, T. Katsuta, M. Watanabe, S. Li, T. Oda, T. Ogawa, and K. Mizuno, Rev. Sci. Instrum. **68**, 1028 (1997).
[28] W. Demtröder, *Laser Spectroscopy* 2nd ed. (Springer, New York, 1996).
[29] C. W. T. Chien, R. E. Bardsley, and F. W. Dalby, Can. J. Phys. **50**, 116 (1972).
[30] P. F. Little and A. von Engel, Proc. R. Soc. London, Ser. A **224**, 209 (1954).
[31] S. Namba, D. Andruczyk, K. Takiyama, D. Ueno, S. Furukawa, and B. W. James, Jpn. J. Appl. Phys. **45**, 8099 (2006).